

Ultrasonic Assisted Turning: A Comparative Study of Surface Integrity



Varun Sharma, Pulak M. Pandey, Uday S. Dixit, Anish Roy
and Vadim V. Silberschmidt

Abstract The surface integrity of machined sample has detrimental effects on the product's life. The machining parameters have been found to significantly affect the surface integrity during the turning operation. Surface roughness, residual stresses and microhardness are the most commonly used parameters to study the surface integrity. In this chapter, an attempt has been made to present a comparative analysis of conventional turning (CT) and ultrasonically assisted turning (UAT) processes with plain and textured cutting tools. The effect of ultrasonic power (measured in terms of amplitude) on surface roughness has been studied during UAT process. An increase in the amplitude improved the surface finish of the machined specimen, significantly. The surface residual stresses generated in the machined part during UAT have been compared for plain and self-lubricating cutting inserts using XRD analysis. An attempt has been made to evaluate the residual stresses generated during the process by using commercially available finite element method package, ANSYS. The generation of a large compressive residual stresses during UAT process with self-lubricating cutting inserts signifies

V. Sharma

Department of Mechanical Engineering, BITS Pilani, Pilani, India
e-mail: varun.sharma@pilani.bits-pilani.ac.in

P. M. Pandey (✉)

Department of Mechanical Engineering, IIT Delhi, New Delhi, India
e-mail: pmpandey@mech.iitd.ac.in

U. S. Dixit

Department of Mechanical Engineering, IIT Guwahati, Guwahati, India
e-mail: uday@iitg.ernet.in

A. Roy · V. V. Silberschmidt

Wolfson School of Mechanical and Manufacturing Engineering, Loughborough University,
Loughborough, UK
e-mail: A.Roy3@lboro.ac.uk

V. V. Silberschmidt

e-mail: v.silberschmidt@lboro.ac.uk

© Springer Nature Singapore Pte Ltd. 2018

S. S. Pande and U. S. Dixit (eds.), *Precision Product-Process Design and Optimization*, Lecture Notes on Multidisciplinary Industrial Engineering,
https://doi.org/10.1007/978-981-10-8767-7_13

better fatigue life of the component. The microhardness measurements are used to demarcate the Machine Affected Zone (MAZ) for UAT and CT process. A comparative analysis between CT and UAT has also been presented in terms of surface integrity to demonstrate better machining regime found in UAT using self-lubricating cutting inserts.

Keywords Surface integrity · Vibration · Conventional turning
Ultrasonic assisted turning · Self-lubricating inserts

1 Introduction

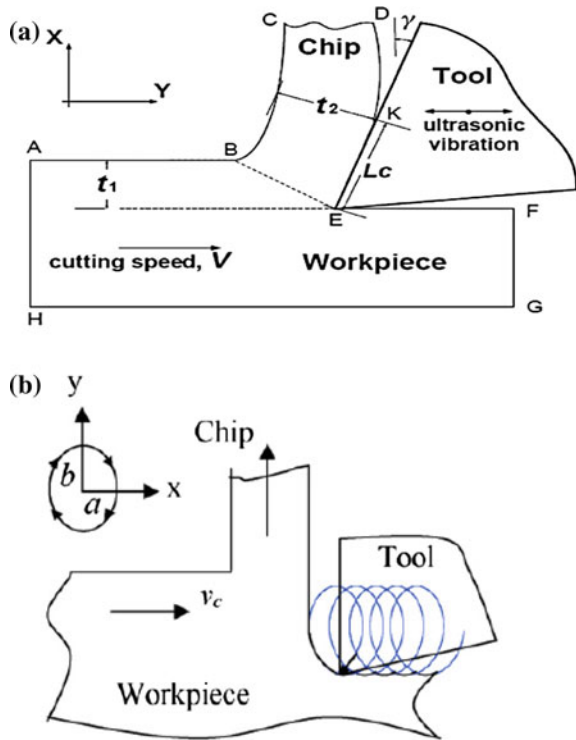
High cutting forces are generated during machining of difficult-to-cut materials. These forces are said to have detrimental effects not only on cutting tool life but also on surface integrity of the machined specimen. Research in recent past has been focused on eliminating adverse impacts of the use of lubricants and coolants. Thus, in order to reduce the carbon footprints of machining, dry machining is preferred (Dixit et al. 2012; Sharma and Pandey 2016e). Researchers have also observed that application of high-intensity ultrasonic power causes a favourable reduction in machining forces. This is often attributed to reduction in material hardness due to acoustic softening (Siddiq and Sayed 2011; Maurotto et al. 2012). This effect of ultrasonic vibrations on hard-to-cut materials is useful in turning, drilling and milling operations.

The work reported in this chapter primarily focuses upon presenting a comparative analysis between CT and UAT process by primarily focussing on the surface integrity (surface roughness, microhardness and residual stresses) of the machined specimen. In the following sections, a brief introduction to UAT process has been presented followed by the research done so far, in this regard.

2 Ultrasonic Assisted Turning

From a review of the literature, ultrasonic-vibration assisted machining of metals first started in the late 1950s (Skelton 1969; Brehl and Dow 2008). Over the years, ultrasonically assisted turning (UAT) has been improved upon significantly. In UAT, high-frequency and low-amplitude vibrations are superimposed on the cutting tool. This vibratory tool movement, in turn, allows for a periodic separation between rotating workpiece and tool. The tool movement may be in one direction (1D-UAT; Fig. 1a), or in a combination of two directions (2D-UAT; Fig. 1b) to yield linear or elliptical motions of cutting edge, respectively (Sharma 2017).

Fig. 1 Schematic representing relative movement of tool and workpiece for **a** 1D-UAT (Patil et al. 2014), **b** 2D-UAT (Nath et al. 2009)



The following paragraphs highlight the schematic of 1D-UAT and 2D-UAT setups developed by various researchers and the mechanism involved in UAT process, which makes it a better alternative to CT for machining of hard-to-cut materials.

2.1 One-Dimensional UAT

One-dimensional UAT (1D-UAT) was introduced in late 1950s and was introduced for machining materials that could not be easily turned using a diamond cutting tool. In the mid-1980s 1D-UAT was used to machine steel, glass and brittle ceramics. It was observed that 1D-UAT lead to better surface integrity. Research in 1D-UAT gained popularity with the advent of difficult-to-cut materials like Ni- and Ti-based alloys. 1D-UAT involves the use of piezoelectric or magnetostrictive actuator to create a reciprocating harmonic motion of high-frequency and low-amplitude vibrations. A suitably shaped acoustic booster and horn is generally used to amplify this ultrasonic motion (Sharma 2017). The cutting tool is then attached to the end of the horn as shown in Fig. 2. The amplitude at the horn end varies from 3 to 20 μm .

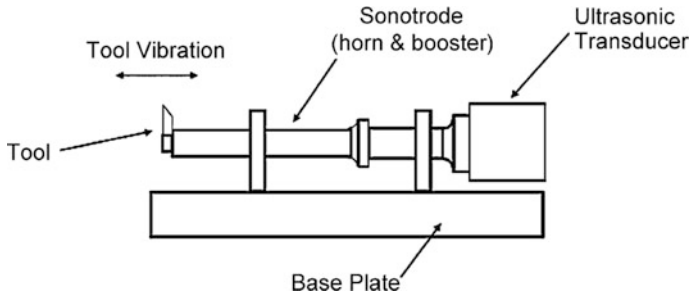


Fig. 2 One-dimensional ultrasonic assisted turning setup (Brehl and Dow 2008)

2.2 Two-Dimensional UAT

Two-dimensional UAT (2D-UAT) was introduced in the 1990s to achieve enhanced force reduction and improved surface finish beyond 1D-UAT. This process adds the vertical harmonic motion to the horizontal motion produced by 1D-UAT. The superimposition of two motions leads to an elliptical motion of the cutting insert. The vibrational amplitude in each axis may or may not be same and is defined as the amplitude of vibration in major axis (A) \times amplitude of vibration along minor axis (B). It is represented as $A \mu\text{m} \times B \mu\text{m}$ (Sharma 2017).

2.3 Resonant Two-Dimensional UAT Systems

The resonant 2D-UAT system creates circular or elliptical motion by making the supporting structure to vibrate at a resonant frequency. By mounting the centre of mass of tool away from midpoint, a two-dimensional motion may be achieved. Brinksmeier and Gläbe (1999) found a bending vibration of supporting structure in direction of depth of cut. When this mode of vibration was combined with horizontal mode of vibration, an elliptical tool path was obtained. Moriwaki and Shamoto (1995) developed resonant 2D system as shown in Fig. 3. The piezoelectric actuators attached to beam side face produced a bending in horizontal and vertical directions on activation. The combination bending motions produced by vibrations resulted in an elliptical path of tool attached at the opposite end.

2.4 Non-resonant 2D-UAT Systems

In this variant of 2D-UAT, a sinusoidal voltage signal applied to piezo actuators resulted in an expansion and contraction of piezoelectric crystals. This motion was then converted to an elliptical motion of the tool with the help of mechanical

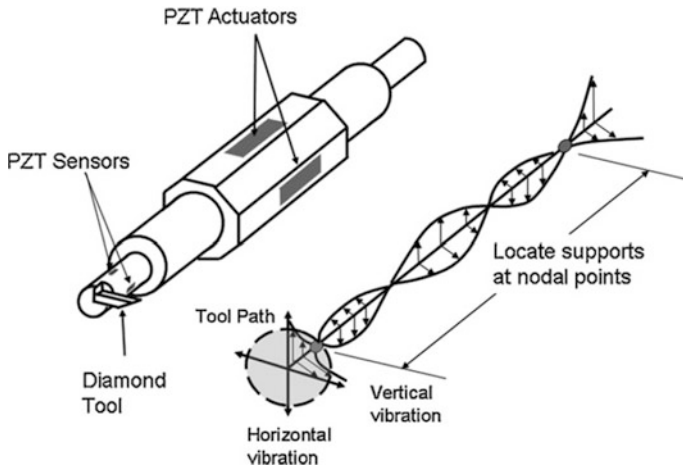


Fig. 3 Resonant 2D system (Brehl and Dow 2008)

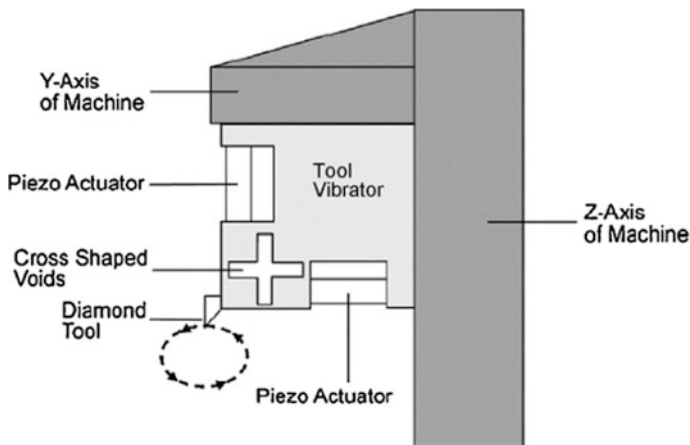


Fig. 4 Non-resonant 2D system (Brehl and Dow 2008)

linkages. The piezoelectric actuators were oriented at a right angle to each other. The tool was mounted on one side of the cross-shaped flexure to limit the crosstalk between two tool motions (Fig. 4). Crosstalk is the transfer of energy back and forth between two modes that results in a distorted tool path in resonant 2D-UAT systems. In order to reduce this effect, phase difference is provided by designing an internal cross-shape which in turn results in an elliptical tool path.

From the above illustrations, it can be deduced that in 1D-UAT, there occurs a linear motion of the cutting insert, whereas an elliptical motion of the cutting insert occurs in 2D-UAT process. The present research attempt has been focused on

enhancing the efficacy of dry UAT process by combining the dual benefits of intermittent cutting of UAT and lubrication of textured cutting insert. The following subsection highlights the processing mechanism of 1D-UAT process.

3 Mechanism of 1D-UAT Process

The mechanism of UAT may be divided into four stages during a single cycle of vibration as shown in Fig. 5 (Patil et al. 2014). In stage 1, cutting tool approaches workpiece material, while in stage 2, the cutting tool makes contact with workpiece. The tool is in full contact with workpiece and starts penetrating into workpiece in stage 3.

When highest level of stress is achieved, it marks maximum penetration depth attained by cutting tool. This stage of UAT is similar to a conventional turning (CT) process as tool is in full contact with workpiece. In the last stage, i.e. in stage 4, the direction of cutting tool is reversed and the tool disengages from the workpiece. This stage of UAT results in a reduction of stress level attained in workpiece. Thus, the stress is variable in UAT, ranging from the maximum in stage 3 to quite less in other stages. As a result, a reduction in the average cutting force is obtained.

Vivekananda et al. (2014) highlighted that for intermittent cutting to occur the following conditions must satisfy:

$$v_C > V, \quad (1)$$

where v_C represents critical cutting speed and V denotes cutting speed. These parameters may be calculated using the following equations:

$$v_C = 2\pi af \quad (2)$$

$$V = \pi DN \quad (3)$$

where a is amplitude and f represents frequency of vibration, D is diameter and N denotes rotational speed of workpiece.

The following paragraphs discuss the research attempts by various researchers pertaining to the surface roughness and residual stresses during conventional and ultrasonic assisted turning processes (Sharma 2017).

3.1 Studies on Surface Roughness

Wang and Zhao (1987) were the pioneers in studying the surface roughness by providing ultrasonic vibration to cutting tool. It was reported that UAT results in an

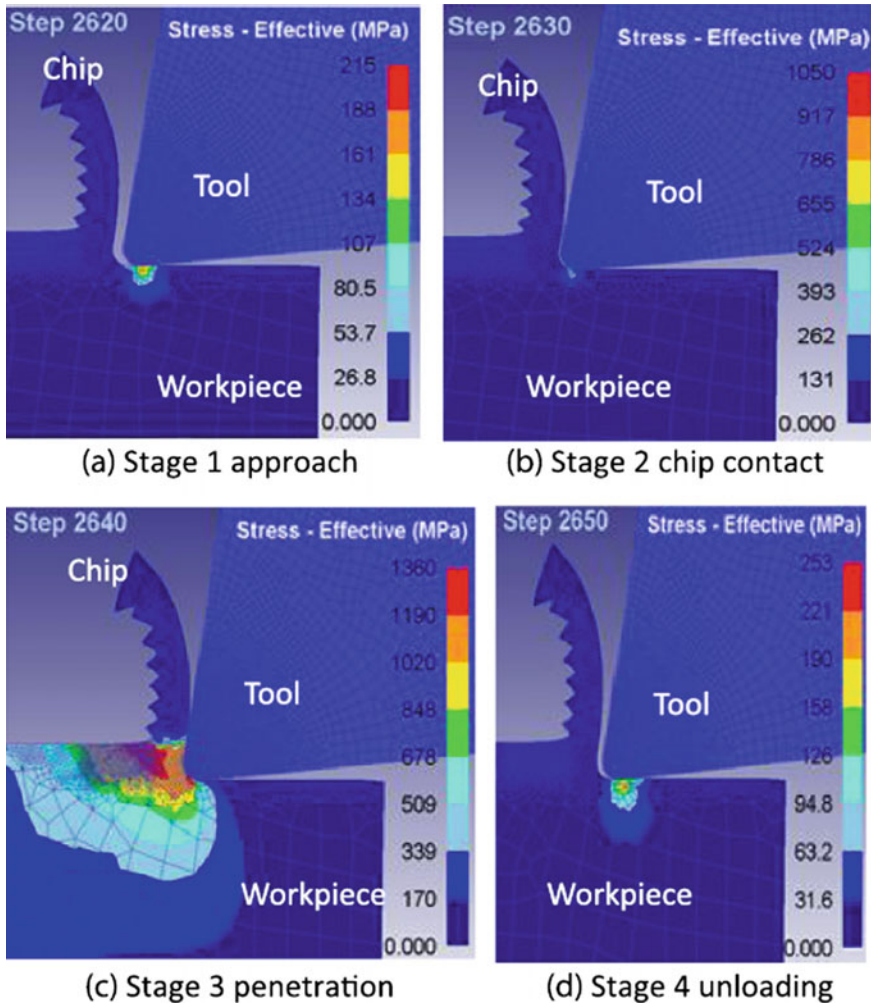


Fig. 5 The schematic representation of four-stage mechanism followed by UAT (Patil et al. 2014)

improvement of the surface finish over CT process. Silberschmidt et al. (2014) reported a twofold improvement in roughness value of Inconel 718 and Ti 15-3-3-3 by UAT when compared to CT. A reduction in chatter and a stable cutting mechanism were observed that resulted in a centre line average surface roughness, R_a , of 0.505 μm during machining Inconel 718 with UAT.

Muhammad et al. (2014) reported 50% improvement in R_a value of $(\alpha + \beta)$ Ti-based alloys. In another research attempt, Nath et al. (2007) found low feed rate to help in attaining better surface finish during UAT. Gao et al. (2002) reported tool tip to be located lower than rotating centre of workpiece by approximately three times the amplitude of vibration, in order to have less ripples formation. A surface

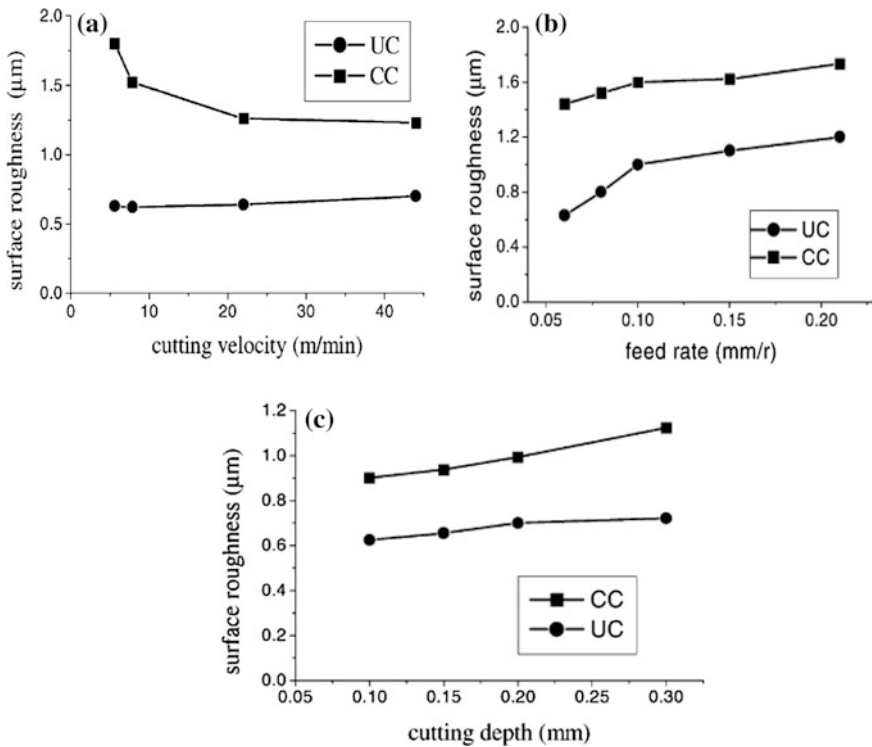


Fig. 6 Variation of surface finish with **a** cutting velocity; **b** feed rate; **c** cutting depth (Gao et al. 2002) (CC conventional cutting; UC ultrasonic cutting)

roughness of order of 30% less was found in machined specimen by providing ultrasonic vibration to cutting tool (refer Fig. 6).

In another research attempt, Lin and Zhong (2006) studied the effects of ultrasonic and cutting parameters on roughness value. The authors reported that high amplitude (3.7 μm) decreased surface roughness by 15% with reference to surface roughness obtained by UAT with an amplitude of 2.2 μm (Fig. 7).

Patil et al. (2014) related improvement in roughness with tool workpiece contact ratio (TWCR). The study indicates optimum cutting velocity, which provided best surface finish. At cutting velocity of 20 m/min, 40% improvement in surface finish could be achieved during UAT of Ti6Al4 V. However, average surface roughness was observed to increase with a further increase in cutting speed (refer Fig. 8).

Fig. 7 Surface roughness variation for cutting and vibration parameters for aluminium-based composite material (Lin and Zhong 2006)

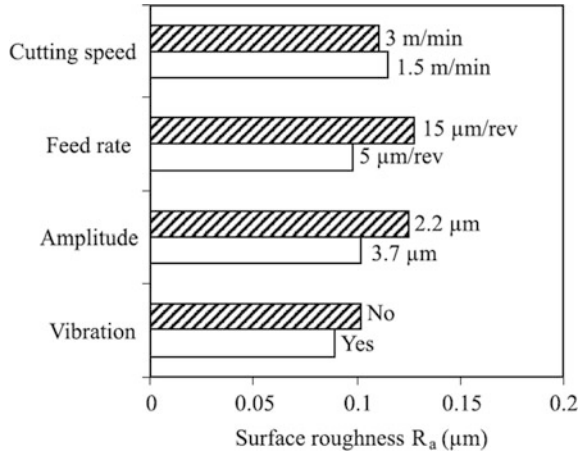
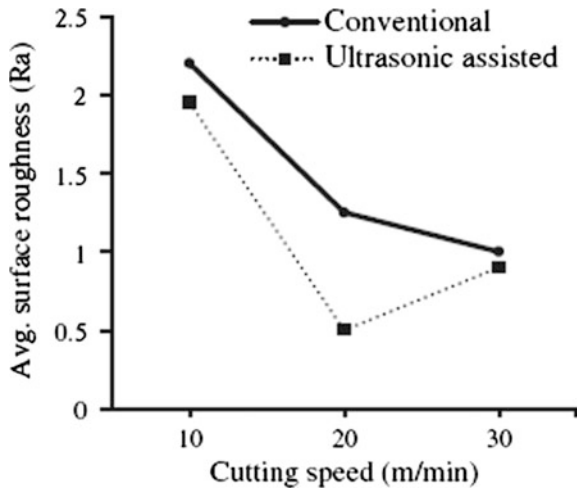


Fig. 8 Effect of cutting speed on surface roughness (Patil et al. 2014)



3.2 Studies on Residual Stresses

Ahmed et al. (2006) measured residual stresses and hardness using nanoindentation tests (Fig. 9). The machined specimens of CT and UAT were held in a plastic mould and a number of indentations were made along the depth of the machined specimen. In Fig. 9, the middle region indicated by ‘plastic’ implies the hardness of plastic mould and is to be ignored in the analysis. It was found that average hardness of the hardened layer in UAT was 60% less than that found during CT of machined part.

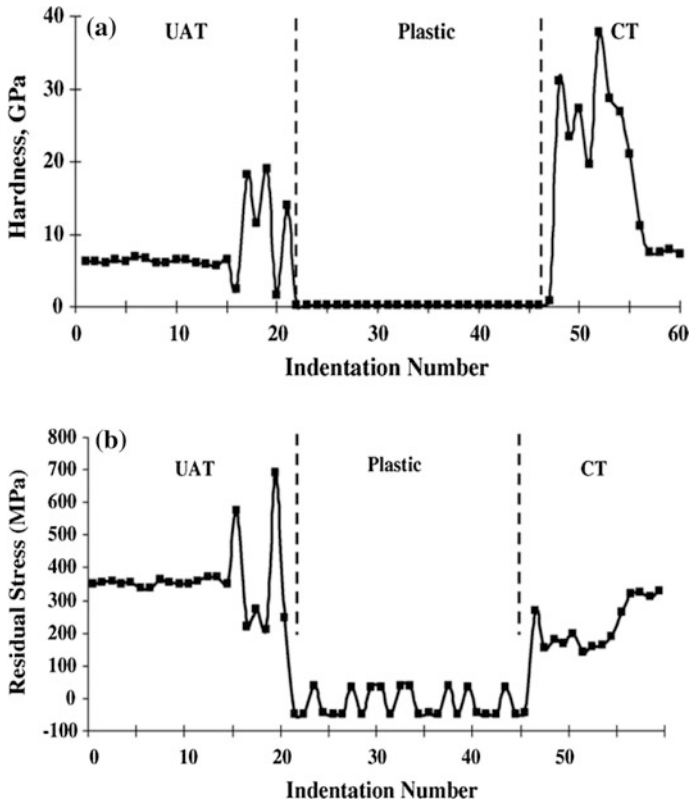


Fig. 9 Variation in **a** hardness and **b** residual stresses for UAT and CT process (Ahmed et al. 2006)

Numerical studies using the Johnson–Cook material model revealed that a high value of compressive residual stresses in UAT is generated as compared to CT (Fig. 9b).

In another research attempt, Silberschmidt et al. (2014) observed an increase in hardness of the surface layer with variation in depth of cut (Fig. 10). It was found that hardness of the CT machined part varied from the bulk (un-machined part). Besides this, since in UAT, the strain rate is expected to be high (when compared to CT), the hardness should have been more; however, Fig. 10 shows the reverse effect. This indicates that the strain rate was not the only factor that affected hardness of machined specimen.

Nestler and Schubert (2014) applied ultrasonic vibrations in radial direction to generate compressive residual stresses in machined part as compared to vibrations in cutting direction. Interestingly, ultrasonic vibration in the feed direction had no effect on residual stresses (Fig. 11).

Fig. 10 Surface hardness variation in CT and UAT (Silberschmidt et al. 2014)

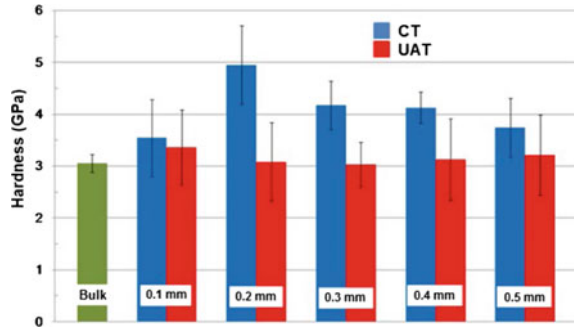
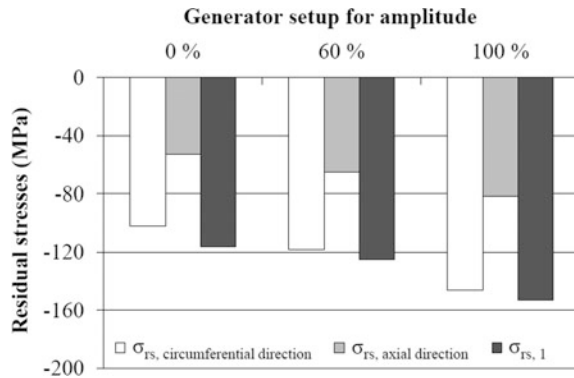


Fig. 11 Amplitude effect on generation of residual stresses in UAT (Nestler and Schubert 2014)



To further enhance efficacy of dry UAT process, the intended research attempts to use self-lubricating textured cutting inserts during UAT process. Sharma and Pandey (2016a, b, c), Sharma et al. (2016) discussed the benefits of self-lubricating cutting insert during UAT process. UAT with self-lubricating cutting inserts resulted in minimum cutting forces accompanied with better surface finish as compared to plane cutting insert. The most favourable method of enhancing the fatigue life is by inducing compressive residual stresses. The present chapter focuses on studying the surface integrity during conventional turning with plain tool (PCT) as well as textured tool (TCT). Surface roughness, residual stress and microhardness measurements at the machined specimen cross section have been taken as criteria for studying the surface integrity of machined specimen.

4 Fabrication of Ultrasonically Assisted Turning Setup

Figure 12a shows the schematic of UAT setup fabricated for the experimentation. The most crucial part in the setup fabrication has been the development of ultrasonic horn (Fig. 12b). The ultrasonic vibratory tool assembly comprised an ultrasonic generator, piezoelectric crystals, booster and a customized horn. The

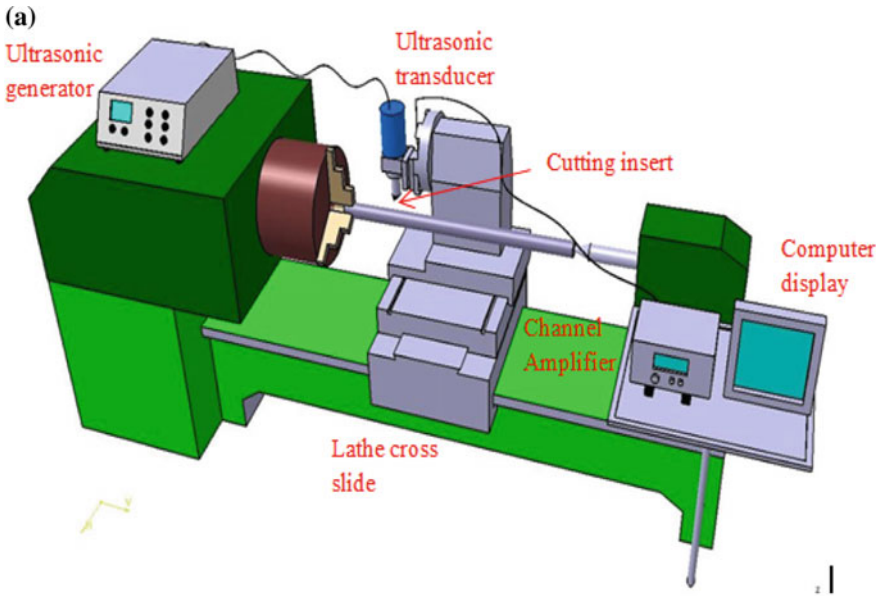


Fig. 12 a Schematic and b actual setup for UAT experimentation (Sharma and Pandey 2016d)

ultrasonic generator (make: Chromtech, Taiwan) generated electrical signals (1200 W, 20 kHz), which were then converted into mechanical vibrations through a stack of piezoelectric crystals. A customized stepped horn (Fig. 13a) was manufactured to boost the vibrations. The ultrasonic generator (Make: Chromtech,

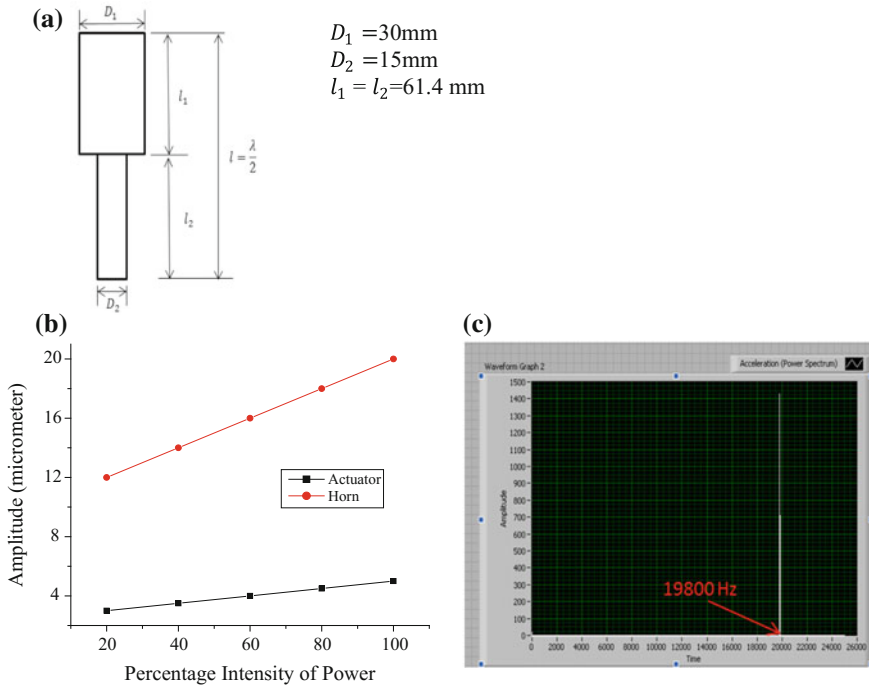


Fig. 13 a Schematic of stepped horn; b calibration of amplitude with percentage intensity of ultrasonic power; c natural frequency of stepped horn using accelerometer (Sharma 2017)

Taiwan) used for present experimentation operated at a frequency of 20 kHz and was with a variable power output source having maximum supply of 1200 W.

In order to analyze the modal and harmonic analysis of the stepped horn, a commercially available FE package, ANSYS was used. The modal analysis revealed that the 12th mode of vibration corresponded to the longitudinal mode with a natural frequency of 19.8 kHz.

Figure 13b shows the calibration graph of amplitude with the percentage intensity of ultrasonic power varied with the ultrasonic generator. Figure 13c presents the frequency of the horn measured using accelerometer. It could be inferred that the horn had a natural frequency of 19.8 kHz.

The developed horn was then mounted on the dynamometer with the help of a fixture. In order to prevent the resonance of fixture with the Kistler dynamometer, the natural frequency of the fixture was measured using hammer test. The maximum third natural frequency of the fixture was around 1000 Hz, which was far less than the natural frequency of the Kistler dynamometer, i.e. 3.2 kHz. Thus, the condition of resonance could be prevented during machining.

4.1 Work Material

4340 hardened steel of dimensions 40 mm in diameter and 400 mm in length has been used as the workpiece material. The elemental composition of the material as measured by EDX analysis is 0.4%C, 1.05%Ni, 1.05%Cr, 0.65%Mn, 0.21%Si and rest Fe. The material hardness was constant with a variation of ± 1 HRC throughout the cross section of the cylindrical workpiece.

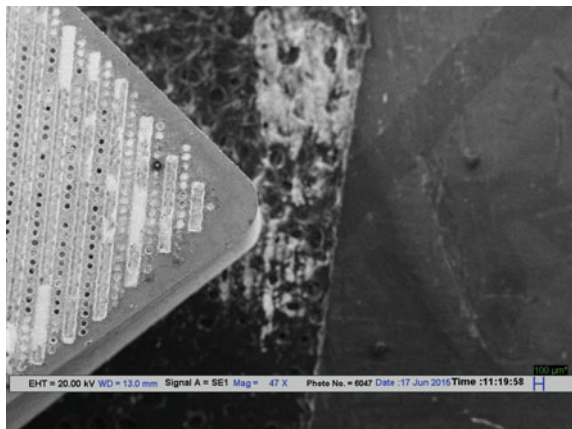
4.2 Cutting Tools

CNMA 120404 THM was used for performing the turning experiments. The selection of this cutting insert was made due to its lack of chip breaker or coating, which facilitated an easy manufacture of a textured pattern. In order to create texture pattern, femtosecond pulsed Nd-YAG laser (wavelength = 1064 nm, pulse energy = 25 MJ, repetition rate = 20 kHz) was used. After texturing, the cutting inserts were cleaned in an ultrasonic acetone bath for 20 min. Figure 14 shows the SEM image of developed textured pattern filled with CaF_2 solid lubricant under microscopic observation.

4.3 Sample Preparation

The machined workpiece was cut into sample size of 10 mm \times 5 mm \times 5 mm using wire-cut EDM. This method was used for the sample preparation, as it resulted in least heat affected zone (HAZ) and thus, facilitated accurate readings for microhardness profiles.

Fig. 14 SEM image of the textured cutting insert ($47\times$ and $100\ \mu\text{m}$ scale) used for present experimentation



4.4 Microhardness Test

For microhardness measurement, cold mounting of samples was performed using a resin powder. The samples were then polished using waterproof SiC paper with grit size ranging from 200 to 1200. The microindentation was measured at a depth of 15, 30, 45, 60, 70, 90, 150 and 300 μm from machined surface to bulk of specimen.

4.5 Measurement of Residual Stress

Among the different techniques that are available for the measurement of residual stresses, XRD is preferred. This is due to the high spatial resolution of XRD accompanied with the measurement in all crystalline materials (Sharma and Pandey 2016d).

In the present work, Panalytical X’pert XRD unit has been used to evaluate the residual stresses with $\sin^2\Psi$ technique. The XRD system was calibrated with respect to the stress-free sample. $\text{CuK}\alpha$ was used as the target material with $\langle 220 \rangle$ plane. The other parameters for the measurement can be found elsewhere in other publications of present researchers (Sharma and Pandey 2016d).

The three-dimensional strain tensor is represented as follows:

$$\epsilon_{ij} = \begin{bmatrix} \epsilon_{11} & \epsilon_{12} & \epsilon_{13} \\ \epsilon_{21} & \epsilon_{22} & \epsilon_{23} \\ \epsilon_{31} & \epsilon_{32} & \epsilon_{33} \end{bmatrix}. \tag{4}$$

For calculating the stress tensor, Hooke’s law is used, providing

$$\sigma_{ii} = \frac{E}{1 + \mu} \epsilon_{ii} + \frac{\mu E}{[(1 + \mu)(1 - 2\mu)]} \Delta, \tag{5}$$

$$\sigma_{ij} = \frac{E}{1 + \mu} \epsilon_{ij}, \tag{6}$$

$$\Delta = \frac{dV}{V} = \sum_{i=1}^3 \epsilon_{ii}. \tag{7}$$

As per the ASTM standard, the stress components are represented by the tensor σ_{ij} given as follows:

$$\sigma_{ij} = \begin{bmatrix} \sigma_{11} & \tau_{12} & \tau_{13} \\ \tau_{21} & \sigma_{22} & \tau_{23} \\ \tau_{31} & \tau_{32} & \sigma_{33} \end{bmatrix}. \tag{8}$$

The stress strain relationship in any direction of a component with respect to the azimuth ϕ (φ) and polar angle ψ (Ψ) is defined as follows (Sharma and Pandey 2016d):

$$\begin{aligned} \epsilon_{\varphi\Psi}^{hkl} = & \frac{1}{2} s_2^{hkl} [\sigma_{11} \cos^2 \varphi \sin^2 \Psi + \sigma_{22} \sin^2 \varphi \sin^2 \Psi + \sigma_{33} \cos^2 \Psi] \\ & + \frac{1}{2} s_2^{hkl} [\tau_{12} \sin(2\varphi) \sin^2 \Psi + \tau_{13} \cos \varphi \sin(2\Psi) + \tau_{23} \sin \varphi \sin(2\Psi)] \cdot \quad (9) \\ & + s_1^{hkl} [\sigma_{11} + \sigma_{22} + \sigma_{33}] \end{aligned}$$

For measuring the residual stress, sample (5 mm × 5 mm × 7 mm) was removed by wire EDM from the cutting length. The samples were then electropolished using 80:20 proportion of perchloric acid and ethanol as the electrolyte.

5 Results and Discussion

The following section highlights the trends in the variation of surface roughness, residual stress and microhardness variation for PCT (CT: Plain tool), TCT (CT: Textured tool), PUAT (UAT: Plain tool) and TUAT (UAT: Textured tool) to analyze the surface integrity.

5.1 Surface Roughness

In order to quantify the surface characteristics produced by CT and UAT, an optical profiler was used. Figure 15 shows the images from the optical profilometer of CT

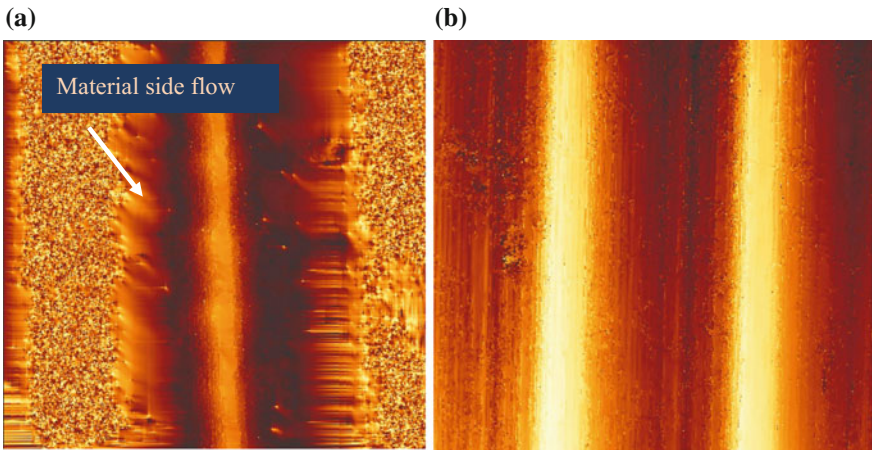


Fig. 15 Images of the machined surface using optical profilometer for **a** PCT; **b** TUAT surface

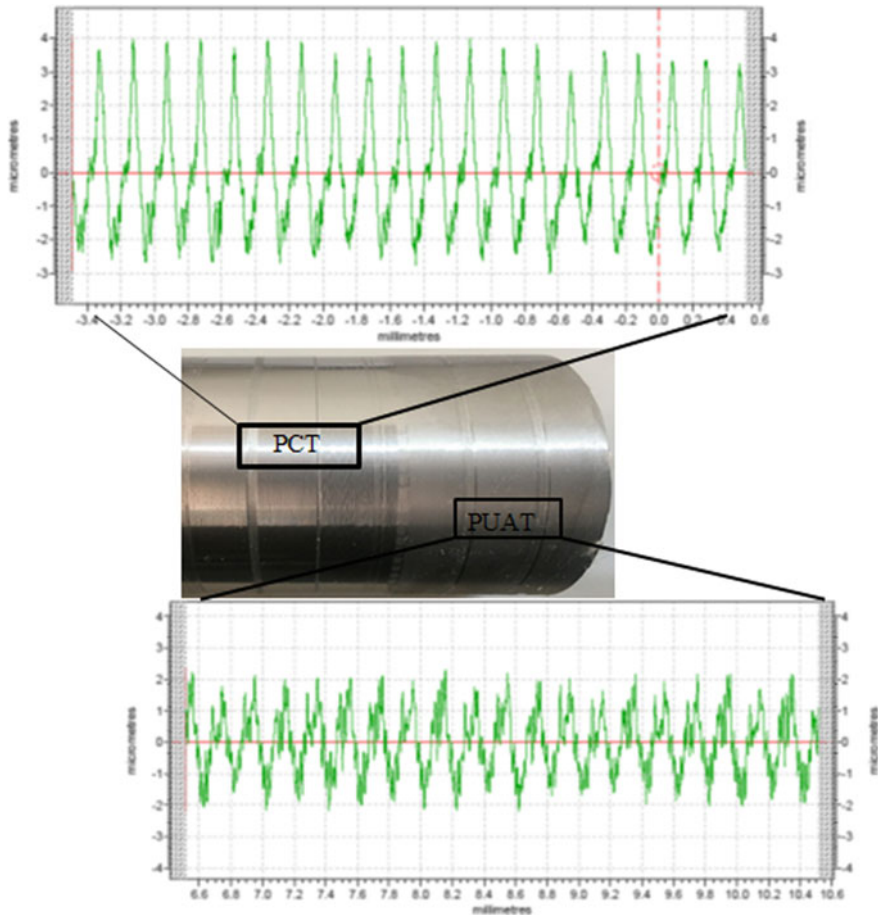


Fig. 16 Machined surface analysis for conventional and ultrasonic assisted turned specimens

and UAT machined specimen. It may be inferred that the material side flow is predominant in CT. This, in turn, resulted in high surface roughness. However, due to the ‘ironing effect’, suppression of material side flow was observed during the UAT process. This decreased the peak-to-valley height, improving surface finish.

Figure 16 shows a clear visual difference between two processes, i.e. CT and UAT. It can be seen that CT process resulted in a glossy finish, whereas matte finish was observed during UAT process. This is in line with the research work of Patil et al. (2014). To further improve the surface finish, UAT with self-lubricating cutting insert was performed.

This technique was found to improve overall surface finish due to a formation of thin layer of lubrication at the tool–chip interface. Essentially, during UAT the penetration of lubricant to inaccessible areas of tool–chip contact is increased with the use of self-lubricating tools, thus reducing the frictional forces (Zou et al. 2015).

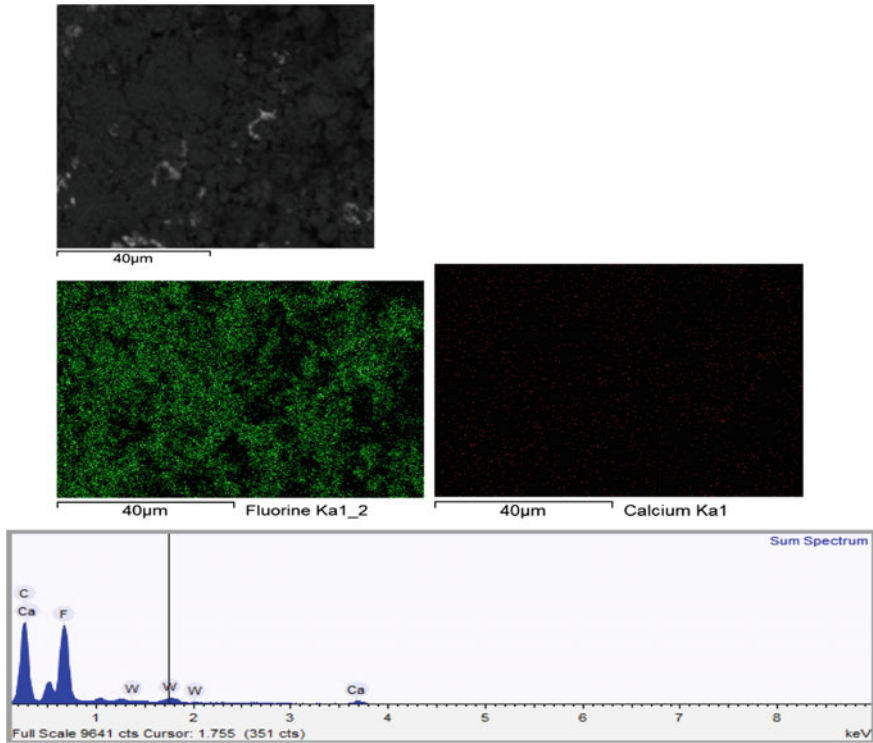


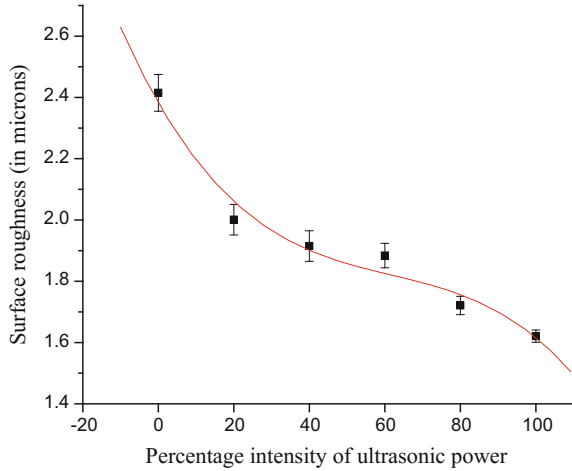
Fig. 17 EDX mapping of textured rake face after 3 min of machining (scale: 40 μm)

Figure 17 shows the EDX map of the top surface of the textured rake face after performing 3 min of cutting under UAT conditions. It can be clearly inferred that Ca and F particles which were earlier embedded into the groove depth had now risen above and formed a thin layer of lubrication on rake face. This, in turn, helped to lower the frictional force between tool and chip back surface. This lubrication of the self-lubricating cutting insert helped to attain better surface finish.

In order to study the effect of increase in percentage intensity of ultrasonic power (i.e. amplitude) on surface roughness, experiments were carried out at constant cutting parameters while varying ultrasonic power. Figure 18 shows the variation in surface roughness values (R_a) for UAT process.

An increase in ultrasonic power leads to a decrease in surface roughness. This is due to the fact that with an increase in the amplitude, the non-contact time of tool with the workpiece decreases, which in turn decreases the TWCR and the cutting forces (Gao et al. 2002).

Fig. 18 Surface roughness variation with percentage intensity of ultrasonic power for PUAT process



5.2 Residual Stress

Figure 19 shows the 2θ plots as measured by Panalytical X’pert Pro stress software for un-machined specimen (M1), conventionally turned specimen (M2), machined specimen with UAT (M3) and machined specimen with self-lubricating cutting insert during UAT process (M4). A gradual shift in the intensity peaks is observed towards the right from M1 to M4. This clearly signifies that with an increase in 2θ angle there occurs a decrease in interatomic plane distance. This, in turn, helps to generate more compressive residual stress. Under same cutting and vibration conditions, UAT with self-lubricating cutting inserts results in more compressive residual stresses as compared to UAT performed with plain tool.

5.3 FEM Modelling

In order to study the surface residual stress, a 2D finite element simulation was carried out. Arbitrary Lagrangian–Eulerian method was used to model the process in a commercially available FE package ABAQUS. The thermo-mechanical properties of material undergoing plastic deformation is assumed to be adequately represented by the Johnson–Cook material model. The constitutive relation of 4340 hardened steel is defined as follows:

$$\bar{\sigma} = \left(A + B\varepsilon_p^n \right) \left[1 + C \ln \left(\frac{\varepsilon}{\varepsilon_0} \right) \right] \left[1 - \left(\frac{T - T_{\text{room}}}{T_{\text{room}} - T_{\text{melt}}} \right)^m \right], \quad (10)$$

where $\bar{\sigma}$ is equivalent stress, A denotes initial yield stress, B represents hardening modulus, ε_p is plastic strain, ε is reference strain rate, ε_0 denotes operating

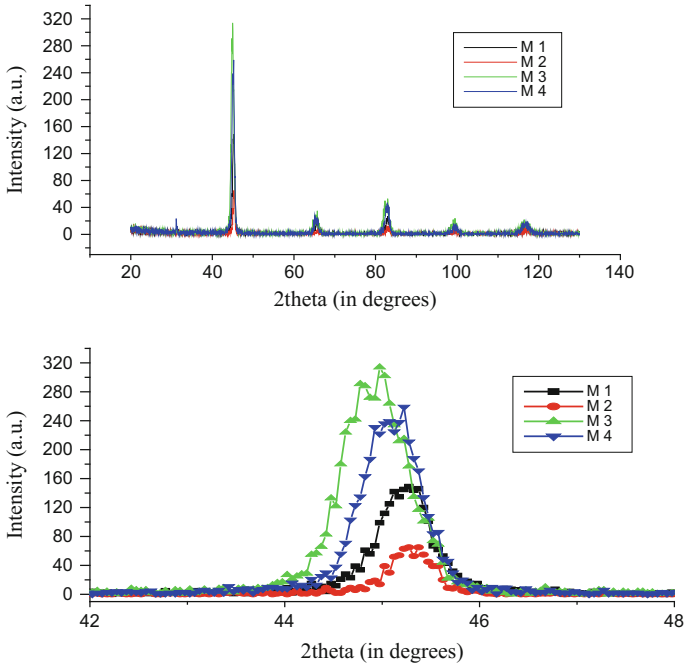


Fig. 19 2θ variation for M1: un-machined, M2: CT, M3: PUAT and M4: TUAT as measured by XRD analysis

temperature, T_{room} is room temperature and T_{melt} denotes melting temperature, C is strain rate coefficient and m is thermal softening coefficient. The Coulomb's law of friction has been used to define the coefficient of friction between tool–chip interface. Four-noded bilinear plane strain quadrilateral (CFE4R) elements with hourglass control and reduced integration were used for meshing the tool and the workpiece. The workpiece was meshed with 12,000 elements with an approximate global size of 0.005 mm, whereas 250 elements with a global size of 0.033 mm were created in the deformable tool. The properties of tool and workpiece used during the simulation process can be found elsewhere (Sharma 2017).

From Fig. 20, it can be inferred that the surface residual stress becomes more compressive in nature during UAT process (c) as compared to CT process (a). Pockets on rake face in a textured tool helps to remove the heat at a faster rate, which results in more compressive residual stress generation in TCT (631.4 MPa) as compared to PCT (899.9 MPa). Moreover, in order to further enhance the fatigue life of the component the superimposition of ultrasonic vibration to textured cutting insert was found to increase compressive residual stress generation in machined specimen (587.1 MPa). The same has been experimentally validated from the shifting of 2θ peaks shown in Fig. 19.

Table 1 presents the experimental conditions for the residual stress measurement during PUAT and TUAT process. It could be inferred that the extent of

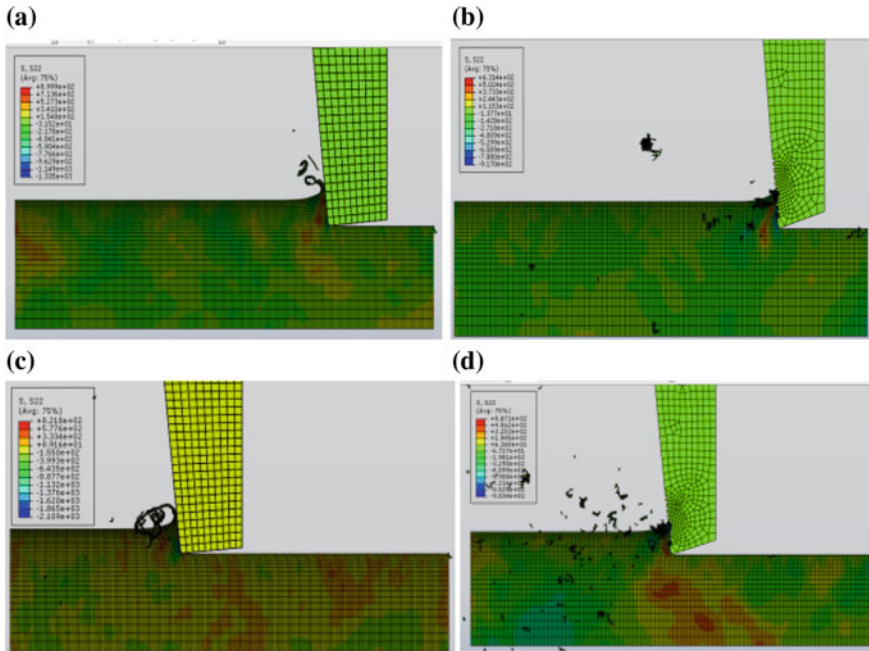


Fig. 20 Residual stress (in MPa) variation in **a** PCT, **b** TCT, **c** PUAT and **d** TUAT

Table 1 Experimental conditions for residual stress measurement

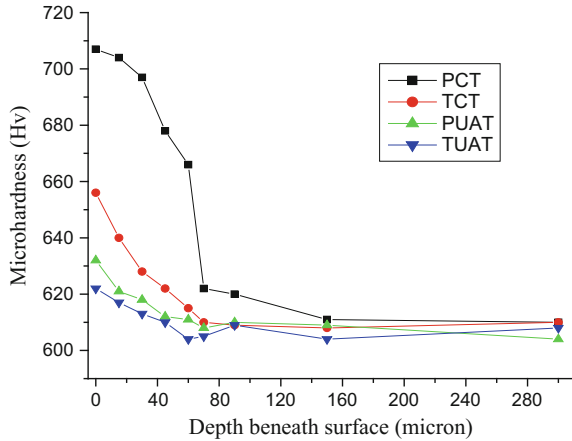
Exp. No.	Depth of cut (mm)	Feed rate (mm/rev)	Cutting speed (m/min)	% intensity of ultrasonic power	Residual stress (MPa)	
					TUAT	PUAT
1.	0.2	0.15	70	40	-123.6	-78.09
2.	0.3	0.20	90	60	256.6	343.00
3.	0.5	0.20	50	60	-239.5	-197.00
4.	0.4	0.25	70	80	-61.7	20.31

compressive residual stress generation was more during TUAT process as compared to PUAT process. The mechanical loading due to UAT combined with cooling effect due to lubrication was used to explain the generation of compressive residual stress in the process.

5.4 Microhardness

Microhardness testing was performed to demarcate the machine affected zone (MAZ) in machined specimen during CT and UAT process. LEICA VM HT AUTO

Fig. 21 Microhardness variation with depth of cut (indentation load = 0.1 kg)



was used for measuring the microhardness variation along the material cross section at 0.1 kg of indentation load. The sample preparation was carried out as discussed in Sect. 2. Figure 21 depicts the microhardness variation along the depth from the machined surface.

From Fig. 21, we observe that the material microhardness reaches the hardness of the bulk specimen after a particular depth of the machined specimen. For PCT, the MAZ is about 60 μ m from the top surface. However, the MAZ decreases to 40 μ m for TCT, PUAT and TUAT turned specimen. This clearly signifies that UAT process is more delicate to the machined specimen as reported by Babitsky et al. (2004). However, the average hardness at the top surface for TUAT process (622 Hv) is 12.86% less than the hardness of PCT turned specimen (702 Hv). This is in line with research work of Babitsky et al. (2004) and Silberschmidt et al. (2014) who proposed less deformed grains in UAT specimen as compared to CT process.

6 Conclusions

A comparative study of conventional and ultrasonic assisted turning with plain and textured tools was carried out. The following conclusions are drawn from the study.

- Ultrasonic assisted turning process generates better surface finish when compared to CT process. An increase in the penetrability of lubricant to tool–chip contact area due to vibration results in better surface finish during ultrasonic assisted turning with textured tool. An improvement in surface finish of the order of 47.5% has been found in PUAT process in comparison to PCT process.

- Ultrasonic assisted turning reduces the tensile residual stresses on the surface, which is helpful for enhancing the fatigue life of the machined component. Sometimes, it may produce compressive residual stresses as well.
- The average hardness of the topmost surface of the machined specimen is less in ultrasonic assisted turning than in CT. It has been found that the average hardness in TUAT process is 12.86% less than PCT process.
- Ultrasonic assisted turning with textured tool results in less MAZ than in CT. One can optimize the cutting and vibration parameters to attain minimum cutting forces accompanied with better surface roughness with ultrasonic assisted turning using self-lubricating cutting inserts.
- The present research has successfully attempted the use of textured cutting inserts during UAT process. This has paved the future research to be intended in the direction of sustainable manufacturing by combining different sustainable techniques like minimum quantity lubrication, cryogenic cooling, etc. in conjunction with UAT process.

Acknowledgements Funding from the engineering and physical sciences research council (UK) through grant EP/K028316/1 and department of science and technology (India) through grant DST/RC-UK/14-AM/2012, project modelling of advanced materials for simulation of transformative manufacturing process (MAST), is gratefully acknowledged. The authors would also acknowledge the help provided by Mr. Shantanab Dinda for his help while performing the experimentation.

References

- Ahmed, N., A.V. Mitrofanov, V.I. Babitsky, and V.V. Silberschmidt. 2006. Analysis of material response to ultrasonic vibration loading in turning Inconel 718. *Materials Science and Engineering A* 424 (1–2): 318–325.
- Babitsky, V.I., A.V. Mitrofanov, and V.V. Silberschmidt. 2004. Ultrasonically assisted turning of aviation materials: Simulations and experimental study. *Ultrasonics* 42: 81–86.
- Brehl, D.E., and T.A. Dow. 2008. Review of vibration-assisted machining. *Precision Engineering* 32 (3): 153–172.
- Brinksmeier, E., and R. Gläbe. 1999. Elliptical vibration cutting of steel with diamond tools experimental setup. In *LFM laboratory for precision machining*. Germany: University of Bremen.
- Dixit, U.S., D.K. Sarma, and J. Paulo Davim. 2012. *Environmentally friendly machining*. New York: Springer.
- Gao, G.F., B. Zhao, F. Jiao, and C.S. Liu. 2002. Research on the influence of the cutting conditions on the surface microstructure of ultra-thin wall parts in ultrasonic vibration cutting. *Journal of Materials Processing Technology* 129: 66–70.
- Lin, G., and Z.W. Zhong. 2006. Ultrasonic assisted turning of an aluminium-based metal matrix composite. *International Journal of Advanced Manufacturing Technology* 27: 1077–1081.
- Maurotto, A., R. Muhammad, A. Roy, V.I. Babitsky, and V.V. Silberschmidt. 2012. Comparing machinability of Ti-15-3-3-3 and Ni-625 alloys in UAT. *Procedia CIRP* 1: 330–335.
- Moriwaki, T., and E. Shamoto. 1995. Ultrasonic elliptical vibration cutting. *CIRP Annals—Manufacturing Technology* 44 (1): 31–34.

- Muhammad, R., M.S. Hussain, A. Maurotto, C. Siemers, A. Roy, and V.V. Silberschmidt. 2014. Analysis of a free machining titanium alloy using conventional and ultrasonically assisted turning. *Journal of Materials Processing Technology* 214: 906–915.
- Nath, C., M. Rahman, and S.S.K. Andrew. 2007. A study on ultrasonic vibration cutting of low alloy steel. *Journal of Materials Processing Technology* 192–193: 159–165.
- Nath, C., M. Rahman, and K.S. Neo. 2009. A study on the effect of tool nose radius in ultrasonic elliptical vibration cutting of tungsten carbide. *Journal of Materials Processing Technology* 209 (17): 5830–5836.
- Nestler, A., and A. Schubert. 2014. Surface properties in ultrasonic vibration assisted turning of particle reinforced aluminium matrix composites. *Procedia CIRP* 13: 125–130.
- Patil, P., S. Joshi, A. Tewar, and S.S. Joshi. 2014. Modelling and simulation of effect of ultrasonic vibrations on machining of Ti6Al4V. *Ultrasonics* 54 (2): 694–705.
- Siddiq, A., and T.E. Sayed. 2011. Acoustic softening in metals during ultrasonic assisted deformation via CP-FEM. *Materials Letters* 65: 356–359.
- Silberschmidt, V.V., S.M.A. Mahdy, M.A. Gouda, A. Naseer, A. Maurotto, and A. Roy. 2014. Surface-roughness improvement in ultrasonically assisted turning. *Procedia CIRP* 13: 49–54.
- Sharma, V., and P.M. Pandey. 2016a. Comparative study of turning of 4340 hardened steel with hybrid textured self-lubricating cutting inserts. *Materials and Manufacturing Processes* 31 (14): 1904–1916. <https://doi.org/10.1080/10426914.2015.1127951>.
- Sharma, V., and P.M. Pandey. 2016b. Geometrical design optimization of hybrid textured self-lubricating cutting inserts for turning 4340 hardened steel. *International Journal of Advanced Manufacturing Technology*. <https://doi.org/10.1007/s00170-016-9163-6>.
- Sharma, V., and P.M. Pandey. 2016c. Study of ultrasonic assisted turning of 4340 steel with plane and self-lubricating cutting inserts. In *Proceedings of manufacturing science and engineering conference ASME MSEC2016 June 27–July 1, 2016, Virginia Tech, Blacksburg, USA*. <https://doi.org/10.1115/msec2016-8565>.
- Sharma, V., and P.M. Pandey. 2016d. Optimization of machining and vibration parameters for residual stresses minimization in ultrasonic assisted turning of 4340 hardened steel. *Ultrasonics* 70: 172–182.
- Sharma, V., and P.M. Pandey. 2016e. Recent advances in turning with textured cutting tools: A review. *Journal of Cleaner Production* 137: 701–715.
- Sharma, V., P.M. Pandey, A. Roy, U.S. Dixit. 2016. Study of surface integrity in conventional and ultrasonic assisted turning with self-lubricating cutting inserts. In *6th international & 27th all india manufacturing technology, design and research conference (AIMTDR-2016)*, December 16–18, 2016 at College of Engineering, Pune, Maharashtra, India.
- Sharma, V. 2017. *Experimental investigations and modelling of ultrasonic assisted turning with self-lubricating textured cutting inserts*. Ph.D. thesis, IIT Delhi.
- Skelton, R.C. 1969. Effect of ultrasonic vibration on the turning process. *International Journal of Machine Tool Design and Research* 9: 363–374.
- Vivekananda, K., G.N. Arka, and S.K. Sahoo. 2014. Design and analysis of ultrasonic vibratory tool (UVT) using FEM, and experimental study on ultrasonic vibration-assisted turning (UAT). *Procedia Engineering* 97: 1178–1186.
- Wang, L.J., and J. Zhao. 1987. Influence of surface roughness in turning with ultrasonic vibration tool. *International Journal of Machine Tools Manufacturing* 27: 181–190.
- Zou, P., Y. Xu, Y. He, M. Chen, and H. Wu. 2015. Experimental investigation of ultrasonic-vibration assisted turning of 304 austenitic stainless steel. *Shock and Vibration*. <https://doi.org/10.1155/2015/817598>.